

# PRIMORDIAL MAGNETOGENESIS IN A BOUNCING MODEL WITH DARK ENERGY

MARCUS V. BOMFIM

Centro Brasileiro de Pesquisas Físicas, Rua Dr. Xavier Sigaud 150, Urca, CEP 22290-180, Rio de Janeiro, RJ, Brazil

EMMANUEL FRION 

Department of Physics and Astronomy, Western University, N6A 3K7, London, Ontario, Canada

NELSON PINTO-NETO 

Centro Brasileiro de Pesquisas Físicas, Rua Dr. Xavier Sigaud 150, Urca, CEP 22290-180, Rio de Janeiro, RJ, Brazil and  
 PPGCosmo, CCE, Universidade Federal do Espírito Santo, Vitória, 29075-910, Espírito Santo, Brazil

SANDRO D. P. VITENTI 

Departamento de Física, Universidade Estadual de Londrina, Rod. Celso Garcia Cid, Km 380, 86057-970, Londrina, Paraná, Brazil  
*Version September 10, 2024*

## ABSTRACT

We investigate primordial magnetogenesis within a quantum bouncing model driven by a scalar field, focusing on various non-minimal couplings between the electromagnetic field and the scalar field. We test three cases: no coupling, a Cauchy coupling with gradual decay, and a Gaussian coupling with rapid fall-off. By exploring these scenarios, we assess a wide range of coupling strengths across different scales. The scalar field, with an exponential potential, behaves as pressureless matter in the asymptotic past of the contracting phase, as stiff matter around the bounce, and as dark energy during the expanding phase. Our findings reveal that, among the tested cases, only the Gaussian coupling can explain the generation of primordial magnetic fields on cosmological scales.

## 1. INTRODUCTION

Bouncing models provide an excellent framework for investigating gravitational particle creation, as they necessarily include a time period characterized by strong gravitational fields. Such models can produce scalar and fermionic particles [Celani et al. \(2017\)](#); [Quintin et al. \(2014\)](#); [Scardua et al. \(2018\)](#), baryons [Delgado et al. \(2020\)](#), and primordial magnetic fields (PMF) [Frion et al. \(2020\)](#); [Battefeld and Brandenberger \(2004\)](#); [Salim et al. \(2007\)](#); [Membela \(2014\)](#); [Sriramkumar et al. \(2015\)](#); [Chowdhury et al. \(2016\)](#); [Qian et al. \(2016\)](#); [Koley and Samtani \(2017\)](#); [Chen et al. \(2018\)](#); [Leite and Pavlović \(2018\)](#); [Chowdhury et al. \(2019\)](#); [Barrie \(2020\)](#); [Mota-harf and Singh \(2024\)](#), which may serve as seeds for the magnetic fields observed across various scales [Durrer and Neronov \(2013\)](#); [Beck \(2012\)](#); [Beck and Wielebinski \(2013\)](#); [Minoda et al. \(2019\)](#); [Bray and Scaife \(2018\)](#); [Ade et al. \(2016\)](#); [Chluba et al. \(2019\)](#); [Zucca et al. \(2017\)](#); [Pogosian and Zucca \(2018\)](#); [Saga et al. \(2018a\)](#); [Kawasaki and Kusakabe \(2012\)](#); [Barai and de Gouveia Dal Pino \(2018\)](#).

The creation of primordial magnetic fields has also been explored within the context of non-minimal couplings between electromagnetic fields and scalar fields in

a variety of models [Emami et al. \(2010\)](#); [Adshead et al. \(2016\)](#); [Turner and Widrow \(1988\)](#); [Bamba and Sasaki \(2007\)](#); [Campanelli et al. \(2008\)](#); [Kunze \(2010, 2013\)](#); [Savchenko and Shtanov \(2018\)](#). This paper aims, as a sequence of Ref. [Frion et al. \(2020\)](#), to examine the possibility of producing PMF arising from these electromagnetic-scalar field non-minimal couplings within the framework of a bouncing model. To this end, we adopt the background bouncing model introduced in Ref. [Bacalhau et al. \(2018\)](#). This model features a scalar field with an exponential potential, which is both simple and rich in its implications, as the scalar field behaves as pressureless matter in the asymptotic past of the contracting phase, as stiff matter around the bounce, and as dark energy during a portion of the expanding phase. Furthermore, this model produces scalar and tensor perturbation spectra and amplitudes compatible with observations of the Cosmic Microwave Background (CMB). Notably, quantum effects at the bounce lead to the magnification of scalar perturbations relative to tensor perturbations, a feature that is challenging to achieve with canonical scalar fields, at least within the classical realm.

The non-minimal couplings investigated between the electromagnetic and scalar fields include Gaussian and Cauchy functions of the scalar field. These couplings vary significantly in their effectiveness: Gaussian couplings exhibit a rapid fall-off, while Cauchy couplings decay more slowly, extending their influence over a broader

range. By studying both fast-decaying (Gaussian) and slow-decaying (Cauchy) types, our analysis not only further explores the Gaussian coupling but also provides a comprehensive examination of the effects of different coupling decay rates. While Gaussian couplings have been used in inflationary magnetogenesis scenarios [Tripathy et al. \(2022\)](#), their application to bouncing magnetogenesis has not been explored previously.

We divide the paper as follows: In Sec. 2, we describe the background model, including the scalar and gravitational fields. In Sec. 3, we outline the electromagnetic sector and describe its quantization and vacuum initial conditions. In Sec. 4, we present the two non-minimal couplings studied and perform numerical calculations to obtain the amplitudes of the electric and magnetic field, power spectra, and spectral indices. We also address back-reaction and make comparisons with observations. We conclude and discuss our findings in Sec. 5.

## 2. THE BACKGROUND

In this section, we summarize the minisuperspace canonical quantization of a cosmological model featuring flat, homogeneous, and isotropic spacelike hypersurfaces, coupled with a canonical scalar field that has an exponential potential  $V(\phi) = V_0 \exp(\lambda\kappa\phi)$ , where  $\kappa \equiv 1/M_p \equiv \sqrt{8\pi G_N}$ ,  $G_N$  is the Newton constant, and  $\lambda, V_0$  are free parameters. It is well known that, in this case, all scalar field solutions of the equations of motion in the asymptotic past of the contracting phase behave as a perfect fluid with  $p = w\rho$  and  $w = (\lambda^2 - 3)/3$ , see [Heard and Wands \(2002\)](#). We choose  $\lambda$  such that  $w \approx 0$ , as it is well known that in this case, scalar cosmological perturbations originating from vacuum quantum fluctuations in a dust-dominated cosmological asymptotic past of such bouncing models present an almost scale-invariant spectrum of scalar perturbations, as observed, see [Peter and Pinto-Neto \(2008\)](#).

As the contracting phase evolves, the kinetic term  $\dot{\phi}^2$  increases substantially over the potential term, implying the scalar field behaves like a stiff matter fluid  $p = \rho$  when the model is approaching the classical singularity. In this phase, we can neglect the potential term for the purpose of quantization. This approximation allows us to use the results of Ref. [Colistete Jr et al. \(2000\)](#), which shows that quantum effects can prevent the cosmological singularity. Hence, the model contains a long contracting period which transitions smoothly through a regular bounce to the expanding phase observed today. In the expanding phase, the scalar field evolves to exhibit a brief period during which it acts as a dark energy component. For further details, see [Bacalhau et al. \(2018\)](#).

Let us focus on the bounce phase, during which quantum effects become relevant and the potential energy density of the scalar field  $\phi$  is negligible compared to its kinetic energy density. This condition implies that  $p = \rho$ , corresponding to a “stiff matter” equation of state. The line element is characterized only by the scale factor  $a(t)$  and is given by

$$ds^2 = N^2 d\tau^2 - a^2(\tau) (dx^2 + dy^2 + dz^2). \quad (1)$$

Defining  $\alpha = \ln(a)$ , changing to the dimensionless scalar field  $\phi \rightarrow \kappa\phi/\sqrt{6}$ , and expressing the Planck length as  $l_p \equiv \sqrt{G_N}$ , we can write the Hamiltonian that governs

the dynamics of the scalar field and scale factor as

$$H = N\mathcal{H} = \frac{N}{2l_p e^{3\alpha}} (-\Pi_\alpha^2 + \Pi_\phi^2). \quad (2)$$

Here,  $\Pi_\alpha$  and  $\Pi_\phi$  are the canonically conjugated momenta to  $\alpha$  and  $\phi$ , respectively:

$$\Pi_\alpha = -\frac{l_p}{N} e^{3\alpha} \frac{d\alpha}{d\tau}, \quad (3a)$$

$$\Pi_\phi = \frac{l_p}{N} e^{3\alpha} \frac{d\phi}{d\tau}, \quad (3b)$$

The lapse function  $N$  is a Lagrange multiplier, and the Hamiltonian is constrained to vanish. In the Dirac quantization procedure for constrained systems [Dirac \(1950\)](#), the constraints must annihilate the wave function, leading to

$$\hat{\mathcal{H}}\Psi(\alpha, \phi) = 0. \quad (4)$$

This condition results in the Wheeler-DeWitt equation of the model:

$$\hat{\mathcal{H}}\Psi(\alpha, \phi) = 0 \Rightarrow \left[ -\frac{\partial^2}{\partial\alpha^2} + \frac{\partial^2}{\partial\phi^2} \right] \Psi(\alpha, \phi) = 0. \quad (5)$$

Following Ref. [Colistete Jr et al. \(2000\)](#), we can obtain the quantum bouncing trajectories of the quantum cosmological model using the de Broglie-Bohm quantum theory, which must satisfy the so-called guidance equations (see reference [Pinto-Neto and Fabris \(2013\)](#) for motivations and details):

$$\Pi_\alpha = \frac{\partial S}{\partial\alpha} = -\frac{l_p}{N} e^{3\alpha} \frac{d\alpha}{d\tau}, \quad (6a)$$

$$\Pi_\phi = \frac{\partial S}{\partial\phi} = \frac{l_p}{N} e^{3\alpha} \frac{d\phi}{d\tau}. \quad (6b)$$

The quantum potential, which incorporates quantum effects, is defined as

$$Q(\alpha, \phi) = \frac{e^{3\alpha}}{2R} \left[ \frac{\partial^2 R}{\partial\alpha^2} - \frac{\partial^2 R}{\partial\phi^2} \right]. \quad (7)$$

In the case of homogeneous and isotropic backgrounds, equations (6) remain invariant under time reparametrization. Therefore, in this case, even at the quantum level, different choices of  $N(\tau)$  produce the same space-time geometry for a given non-classical solution.

Equation (5) represents a simple Klein-Gordon equation in minisuperspace, and we can express the general solution as

$$\begin{aligned} \Psi(\alpha, \phi) = & \int F(\bar{k}) \exp[i\bar{k}(\alpha - \phi)] d\bar{k} \\ & + \int G(\bar{k}) \exp[i\bar{k}(\alpha + \phi)] d\bar{k}. \end{aligned} \quad (8)$$

As established in Ref. [Colistete Jr et al. \(2000\)](#), we choose the Gaussian superposition

$$F(\bar{k}) = G(\bar{k}) = \exp \left[ -\frac{(\bar{k} - d)^2}{\sigma^2} \right], \quad (9)$$

which yields the expression

$$\Psi = \sigma \sqrt{\pi} \left\{ \exp \left[ -\frac{(\alpha + \phi)^2 \sigma^2}{4} \right] \exp[i d(\alpha + \phi)] + \exp \left[ -\frac{(\alpha - \phi)^2 \sigma^2}{4} \right] \exp[-i d(\alpha - \phi)] \right\}. \quad (10)$$

We can extract the phase  $S$  from Eq. (10). By inserting this phase into the the guidance Eqs. (6), we obtain the Bohmian trajectories for  $\alpha(t)$  and  $\phi(t)$ , where  $t$  is the cosmic time for which the lapse function is  $N = 1$ . The equations form a planar system represented as follows

$$l_p \dot{\alpha} = \frac{\phi \sigma^2 \sin(2d\alpha) + 2d \sinh(\sigma^2 \alpha \phi)}{2e^{3\alpha} [\cos(2d\alpha) + \cosh(\sigma^2 \alpha \phi)]}, \quad (11a)$$

$$l_p \dot{\phi} = \frac{-\alpha \sigma^2 \sin(2d\alpha) + 2d \cos(2d\alpha) + 2d \cosh(\sigma^2 \alpha \phi)}{2e^{3\alpha} [\cos(2d\alpha) + \cosh(\sigma^2 \alpha \phi)]}. \quad (11b)$$

The dot denotes a derivative with respect to cosmic time  $t$ . This leads to the relation

$$X \equiv \frac{d\alpha}{d\phi},$$

$$= \frac{\phi \sigma^2 \sin(2d\alpha) + 2d \sinh(\sigma^2 \alpha \phi)}{-\alpha \sigma^2 \sin(2d\alpha) + 2d \cos(2d\alpha) + 2d \cosh(\sigma^2 \alpha \phi)}. \quad (12)$$

Figure 1 depicts the phase space formed by  $\alpha$  and  $\phi$ , restricted to solutions with a classical limit. All such solutions have a bounce, occurring along the line  $\phi = 0$ . The classical limit is recovered for large  $\alpha$  (i.e.,  $X \approx \pm 1$  for large  $\alpha$ , as seen in Eq. (12)). Although cyclic solutions also exist, they are not physical because they do not contain a classical limit.

For any solution of the Wheeler-De Witt equation, the guidance equations enable us to find the Bohmian trajectories that describe the evolution of the system. We observe that Bohmian scale factor solutions that contain a classical limit do not exhibit singularities, featuring a bouncing point that connects the contracting phase to the expanding phase.

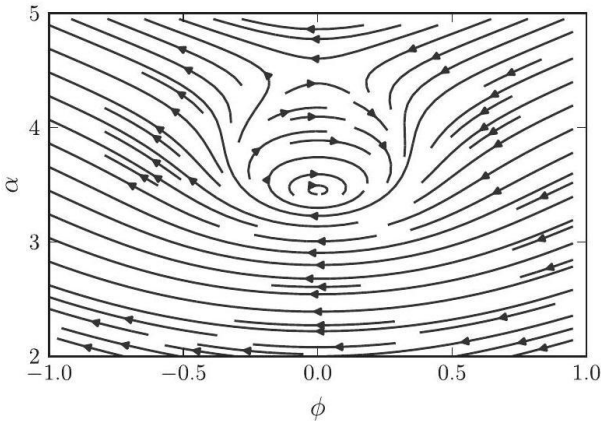


**Figure 1.** Phase space solutions for the system of Eqs. (11) for  $d = -1$  and  $\sigma = 1$ . We notice bouncing solutions and cyclic solutions. Figure taken from reference Bacalhau et al. (2018).

For the numerical calculations, we use the time  $\tau$  defined in Bacalhau et al. (2018) as

$$\alpha = \alpha_b + \frac{\tau^2}{2}, \quad (13)$$

where the bounce occurs at  $\tau = 0$ . This choice of time is computationally more well-suited than cosmic or conformal time since those vary over many orders of magnitude during the evolution of the model. The lapse function  $N$  for this choice of time is

$$N = \frac{\tau}{H}. \quad (14)$$

Where  $H \equiv \dot{a}/a$  is the Hubble parameter, while  $H_0$  will denote its value today.

We calculate the classical limits of Eqs. (11) for large values of  $\alpha$ , specifically at the points where the hyperbolic function dominates. This calculation yields the following relations:

$$X \approx \coth(\sigma^2 \alpha \phi),$$

$$\frac{H}{H_0} \approx \frac{R_H}{l_p} \frac{de^{-3\alpha}}{\coth(\sigma^2 \alpha \phi)},$$

$$l_p \dot{\phi} \approx de^{-3\alpha}.$$

In this approach, Eqs. (11) describe the behavior of any minisuperspace model containing a canonical scalar field, regardless of its potential, since the kinetic term generally dominates around the bounce. This dominance allows for a connection to any classical canonical scalar field with generic potentials, as long as the potential becomes negligible near the bounce.

Reference Bacalhau et al. (2018) investigates a canonical scalar field model with exponential potential which connects the classical behaviour presented in Ref. Heard and Wands (2002) with the quantum evolution described in Ref. Colistete Jr et al. (2000). The model exhibits several interesting features: scalar and tensor perturbations consistent with CMB observations, a kinetic dominated quantum bounce occurring far enough from the Planck scale in order to avoid compromising the Wheeler-DeWitt approach, and a transient dark energy phase during the late expansion. As both the quantum and classical phases present the same stiff matter behaviour at high curvatures, where the potential is negligible, they can be joined together, yielding a complete model contracting from an asymptotically dust-dominated phase in the far past, passing through a quantum bounce when the scalar field has a stiff matter behaviour, and expanding to an era where the scalar field behaves as dark energy, when the potential becomes significant. In order to have these properties, the parameters  $d$ ,  $\alpha_b$ ,  $\sigma$ , and  $\chi_b$  ( $\chi_b$  controlling when the scalar field behaves as dark energy in the expanding phase, see Bacalhau et al. (2018) for details) must lie within a specific domain.

In Fig. 2, we present the evolution of  $\alpha$  with respect to  $\tau$ , alongside the evolution of the scalar field  $\phi$ . From this point onward, we evolve all background and perturbation quantities up to  $\tau = 9.3$ , which corresponds to a moment just before the scalar field begins to behave as dark energy, as determined by the parameters in Table 1. This time is selected to align with our current understanding of the universe, where dark energy currently dominates

the energy budget. Additionally, we limit the evolution to this point to avoid the complexities associated with the dark energy phase, which would require a more intricate treatment of perturbations.

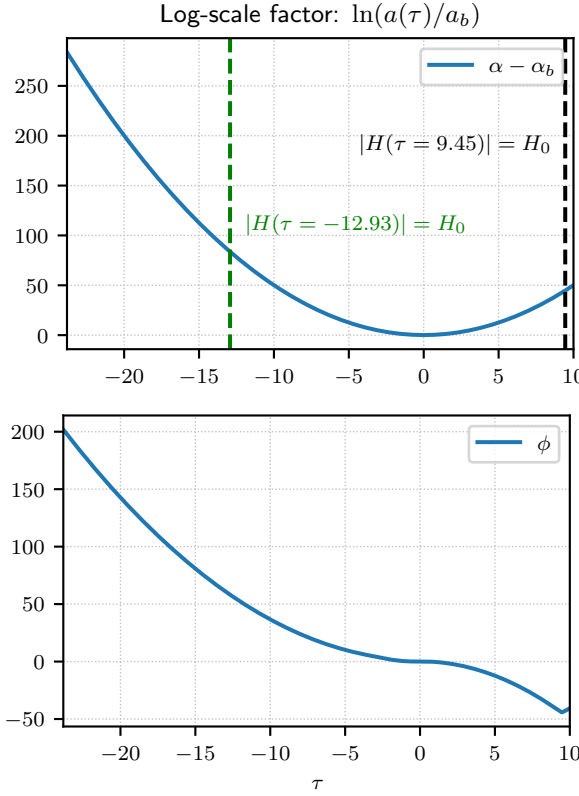


**Figure 2.** Evolution of the number of e-folds  $\alpha - \alpha_b$  with  $\tau$ . The green vertical line marks time during the contraction phase when the Hubble radius is equal to the current Hubble radius. The blue vertical line indicates the same moment during the expanding phase. The scalar field varies within the range  $\approx (-50, 200)$  over the displayed time interval, encompassing most of the relevant scales of the model.

In Bacalhau et al. (2018), we selected two specific sets of parameters, presented in its Table 1, which we also use in this paper. These sets produce physically motivated models, as discussed in the table legend. Having established the background model and its key parameters, we now proceed to investigate magnetogenesis within this framework. All subsequent computations and analyses will be conducted within this bouncing cosmological setting.

### 3. THE ELECTROMAGNETIC SECTOR

#### 3.1. Equations of Motion and Power Spectra

To break the conformal invariance of Maxwell electromagnetism, we introduce a coupling between the electromagnetic field and a scalar field, described by the Lagrangian

$$\mathcal{L} = -f(\phi)F_{\mu\nu}F^{\mu\nu}, \quad (15)$$

where  $f(\phi)$  represents the coupling function. In our analysis, we consider three specific forms: the Gaussian coupling  $f_G(\phi)$ , the Cauchy coupling  $f_C(\phi)$ , and the conformal

	d	$\sigma$	$\alpha_b$	$\chi_b$
Set-1	$-9 \times 10^{-4}$	9	$8.3163 \times 10^{-2}$	$2 \times 10^{36}$
Set-2	$-9 \times 10^{-4}$	100	$7.4847 \times 10^{-3}$	$4 \times 10^{36}$

**Table 1**

Parameter sets for the scalar field-driven bouncing cosmological model that yield primordial perturbations consistent with CMB observations. These parameters determine the scalar amplitude  $\Delta_{\zeta_k}$ , the scalar spectral index, and the tensor-to-scalar ratio  $r$  at horizon crossing. Set-1 produces  $\Delta_{\zeta_k} = 1.4 \times 10^{-10}$  and  $r = 1.9 \times 10^{-7}$ , while Set-2 results in  $\Delta_{\zeta_k} = 4.6 \times 10^{-11}$  and  $r = 1.3 \times 10^{-5}$ . These values match constraints from CMB data, ensuring the viability of the model for early universe predictions. For more details, see Bacalhau et al. (2018).

mal case  $f_0(\phi)$ , given by:

$$f_G(\phi) = \frac{1}{4} + e^{(\gamma_G^2 - \phi^2)/\beta_G^2} \quad (16)$$

$$= \frac{1}{4} + e^{\alpha_G^2 - (\phi/\beta_G)^2} \quad (17)$$

$$f_C(\phi) = \frac{1}{4} + \frac{e^{\alpha_C^2}}{1 + (\phi/\beta_C)^2}, \quad (18)$$

$$f_0(\phi) = \frac{1}{4}. \quad (19)$$

Here,  $\alpha_i$  controls the amplitude and  $\beta_i$  sets the scale for  $i = G, C$ , both treated as free parameters. For the Gaussian coupling, the transition between conformal and non-conformal regimes occurs at  $\phi = \pm\gamma_G = \alpha_G\beta_G$ . The behavior of the Cauchy coupling mirrors the Gaussian one when  $\phi/\beta_C \ll 1$ , but for  $\phi/\beta_C \gg 1$ , the Cauchy function decays more slowly, following a  $1/\phi^2$  pattern, whereas the Gaussian decays exponentially. In Fig. 2, we observe that the scalar field  $\phi$  varies between approximately  $-50$  and  $200$  over the relevant time interval. Consequently, the suppression in the Cauchy coupling remains modest, reaching at most  $(\beta_C/200)^2$ . In order to achieve a significant suppression, a very small  $\beta_C$  is required. Therefore, we set  $\alpha_C = \alpha_G$  and  $\beta_C = \alpha_G\beta_G e^{-\alpha_G^2/2}$  so that both the Cauchy and Gaussian couplings cross into the conformal regime at the same value of  $\phi$  (assuming that  $e^{\alpha_C^2} \gg 1$ ). This choice of parameters aligns the two couplings for a consistent comparison, that is,  $f_G(\alpha_G\beta_G) \approx f_C(\alpha_G\beta_G) \approx 1$ .

The electromagnetic field equations take the form

$$\partial_\mu(\sqrt{-g} f F^{\mu\nu}) = 0, \quad (20)$$

where  $F_{\mu\nu} = \partial_\mu A_\nu - \partial_\nu A_\mu$ , and  $A_\mu$  represents the gauge potential. We work in the Coulomb gauge relative to the cosmic time foliation, setting  $A_0 = 0$  and  $\partial_i A^i = 0$ .

To quantize the electromagnetic field, we expand the operator associated with the spatial part of the vector potential as follows

$$\hat{A}_i(t, \mathbf{x}) = \sum_{\sigma=1,2} \int \frac{d^3 k}{(2\pi)^{3/2}} [\epsilon_{i,\sigma}(\mathbf{k}) \hat{a}_{\mathbf{k},\sigma} A_{k,\sigma}(t) e^{i\mathbf{k}\cdot\mathbf{x}} + \text{H.C.}], \quad (21)$$

where  $\epsilon_{i,\sigma}(\mathbf{k})$  are the two orthonormal and transverse polarization vectors associated with the Coulomb gauge, remaining constant across spatial slices. The comoving

wave vector  $\mathbf{k}$  has a magnitude given by  $k$ , and H.C. denotes the Hermitian conjugate. The operators  $\hat{a}_{\mathbf{k},\sigma}$  and  $\hat{a}_{\mathbf{k},\sigma}^\dagger$  are the annihilation and creation operators, respectively, which satisfy the following commutation relations:

$$[\hat{a}_{\mathbf{k},\sigma}, \hat{a}_{\mathbf{k}',\sigma'}^\dagger] = \delta_{\sigma\sigma'}\delta(\mathbf{k} - \mathbf{k}'),$$

and

$$[\hat{a}_{\mathbf{k},\sigma}^\dagger, \hat{a}_{\mathbf{k}',\sigma'}^\dagger] = 0; [\hat{a}_{\mathbf{k},\sigma}, \hat{a}_{\mathbf{k}',\sigma'}] = 0.$$

The time-dependent coefficients  $A_{k,\sigma}(t)$  and their corresponding momenta  $\Pi_{k,\sigma} \equiv 4af\dot{A}_{k,\sigma}(t)$  must satisfy the vacuum normalization

$$A_{k,\sigma}(t)\Pi_{k,\sigma}^*(t) - A_{k,\sigma}^*(t)\Pi_{k,\sigma}(t) = i, \quad (22)$$

for each  $k$  and  $\sigma$ .

As it is well known, the gauge-fixed electromagnetic field, in the absence of charges, is equivalent to that of two free real scalar fields, corresponding to each polarization direction  $\sigma$ . Since we are considering an isotropic background, we choose a single time-dependent coefficient to describe both polarizations, i.e.  $A_{k,1} = A_{k,2} \equiv A_k$ , which yields the same vacuum for both cases.

Inserting this decomposition into the equations of motion Eq. (20) leads to the following equations for the modes  $A_k(t)$ :

$$\ddot{A}_k + \left( \frac{\dot{a}}{a} + \frac{\dot{f}}{f} \right) \dot{A}_k + \frac{k^2}{a^2} A_k = 0. \quad (23)$$

where in the equation above, dots denote derivatives with respect to cosmic time. We now introduce a set of dimensionless quantities that simplify the analysis

$$Y \equiv \frac{a}{a_0}, \quad A_{sk} \equiv \frac{A_k}{\sqrt{R_H}}, \quad (24)$$

$$x_b \equiv \frac{a_0}{a_b}, \quad k_s \equiv \frac{kR_{H_0}}{a_0}, \quad \eta_s \equiv \int \frac{dt}{R_{H_0}Y}, \quad (25)$$

where  $R_H \equiv R_{H_0}/a_0$  is the co-moving Hubble radius, and  $R_{H_0}$  is the Hubble radius today. Therefore, Eq. (23) turns into

$$A_{sk}'' + \frac{f'}{f} A_{sk}' + k_s^2 A_{sk} = 0, \quad (26)$$

where now the prime indicates a derivative with respect to  $\eta_s$ .

Generally, the Hamiltonian generating the general  $\tau$  evolution ( $dt = N d\tau$ ) of such systems reads

$$\mathcal{H} = \frac{\Pi_{sk}^2}{2m} + \frac{m\nu^2 A_{sk}^2}{2}, \quad (27)$$

It is equivalent to a Hamiltonian describing a harmonic oscillator with time dependent effective mass  $m = af/N$  and frequency  $\nu = Nk_s/a$ . We plot the frequency  $\nu$  along the Ricci scale  $l_R \equiv R^{-1/2}$ , where  $R$  is the Ricci scalar, in Fig. 3. Note that, given our choices of dimensionless variables, all variables with units of distance are expressed in units of the Hubble radius today.

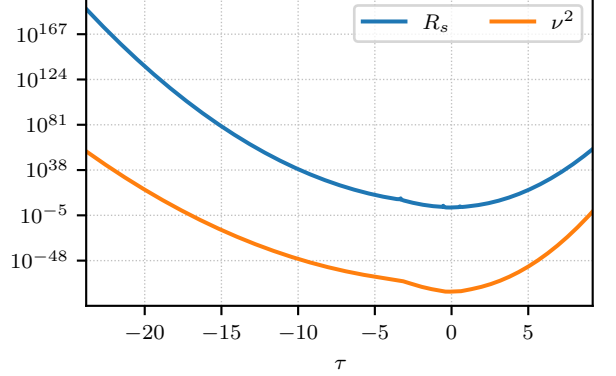


**Figure 3.** Evolution of the frequency  $\nu$  and the Ricci scale with  $\tau$ .

The energy densities of the electric and magnetic fields are respectively given by:

$$\rho_E = \frac{f}{8\pi} g^{ij} \dot{A}_i \dot{A}_j, \quad (28)$$

$$\rho_B = \frac{f}{16\pi} g^{ij} g^{lm} (\partial_j A_m - \partial_m A_j) (\partial_i A_l - \partial_l A_i), \quad (29)$$

where  $g^{ij} = \delta^{ij}/a^2$  represents the spatial components of the inverse metric. To derive the spectral energy densities, we insert expansion (21) into  $\rho_E$  and  $\rho_B$ , thus transforming  $\hat{\rho}_E$  and  $\hat{\rho}_B$  into quantum operators and computing their vacuum expectation values:

$$\langle 0 | \hat{\rho}_B | 0 \rangle = \frac{f}{2\pi^2 R_{H_0}^4 Y^4} \int d\ln k_s |A_{sk}|^2 k_s^5, \quad (30)$$

$$\langle 0 | \hat{\rho}_E | 0 \rangle = \frac{f}{2\pi^2 R_{H_0}^4 Y^4} \int d\ln k_s |A'_{sk}|^2 k_s^3. \quad (31)$$

Defining the spectra as

$$\mathcal{P}_i \equiv \frac{d \langle 0 | \hat{\rho}_i | 0 \rangle}{d\ln k}, \quad i = E, B, \quad (32)$$

we find:

$$\mathcal{P}_B \equiv B_\lambda^2 = \frac{f}{2\pi^2 R_{H_0}^4} \frac{|A_{sk}|^2}{Y^4} k_s^5, \quad (33)$$

$$\mathcal{P}_E \equiv E_\lambda^2 = \frac{f}{2\pi^2 R_{H_0}^4} \frac{|A'_{sk}|^2}{Y^4} k_s^3 = \frac{1}{2\pi^2 R_{H_0}^4} \frac{|\Pi_{sk}|^2}{f Y^4} k_s^3. \quad (34)$$

In the last line, we also expressed  $\mathcal{P}_E$  in terms of the momentum canonically conjugate to the gauge field,  $\Pi_{sk} = f A'_{sk}$ , which is equivalent to the electric field mode itself. Apart from a potential time-dependent coupling, note that both power spectra exhibit the same  $Y^{-4}$  behavior, as expected for an electromagnetic field. Any departure from this behavior must arise from the function  $f$  and the magnitude of the field modes, which only vary if the coupling is not constant.

Finally, we express the magnetic and electric fields,  $B_\lambda$  and  $E_\lambda$ , using  $H_0^2 \approx 1.15 \times 10^{-64}$  G. This conversion from the Hubble radius to Gauss is done to facilitate comparisons with the existing literature, which commonly uses

Gauss as the unit of measurement.

$$B_\lambda = \sqrt{\frac{f}{2\pi^2}} \frac{|A_{sk}|}{Y^2} k^{5/2} 1.15 \times 10^{-64} \text{G}, \quad (35)$$

$$E_\lambda = \sqrt{\frac{1}{2\pi^2 f}} \frac{|\Pi_{sk}|}{Y^2} k^{3/2} 1.15 \times 10^{-64} \text{G}. \quad (36)$$

### 3.2. Vacuum Initial Conditions

In the context of a cosmological bouncing model driven by a scalar field, we define vacuum initial conditions to accurately determine the behavior of the electromagnetic field throughout the bounce and the subsequent expansion phase. Our model considers two types of non-minimal couplings between the electromagnetic field and the scalar field: Gaussian and Cauchy couplings. These couplings may influence the initial conditions and the subsequent evolution of the field modes.

We establish the adiabatic vacuum initial conditions to ensure that each mode of the electromagnetic field starts in its lowest possible energy state within a smoothly varying background. This is a very reasonable assumption, as in the asymptotic past of such models the universe is almost empty and flat, with almost nothing but quantum fluctuations of an almost Minkowski vacuum state for fields and cosmological perturbations. By initializing the field in a vacuum state, we ensure that any electromagnetic fields observed in the expansion phase can be attributed solely to the dynamics of the contraction and bounce, without interference from initial modes. These initial conditions are mathematically expressed in terms of the coupling function  $f(\phi(\eta_s))$ , where  $\phi$  is the time-dependent scalar field in conformal time  $\eta_s$ .

For the electromagnetic field  $A_\mu$  in a cosmological background, the leading order adiabatic vacuum initial conditions are specified as follows:

$$A_k(\eta_s) = \frac{e^{-ik\eta_s}}{\sqrt{2k f(\phi(\eta_s))}}, \quad (37)$$

$$\Pi_k(\eta_s) = f(\phi(\eta_s)) A'_k(\eta_s) = -i \sqrt{\frac{f(\eta_s) k}{2}} e^{-ik\eta_s}. \quad (38)$$

These expressions guarantee that, in the distant past (before the bounce), when the coupling function  $f(\phi) \approx \frac{1}{4}$ , the modes take the form

$$|A_k| = \sqrt{\frac{2}{k}}, \quad (39)$$

$$|\Pi_k| = \sqrt{\frac{k}{8}}. \quad (40)$$

Generically, the adiabatic vacuum initial conditions can be derived using the complex structure approach presented in Ref. Penna-Lima et al. (2023). In this framework, based on the physical idea that the effective frequency of the mode varies much slower than the time scale defined by the frequency itself, the adiabatic vacuum initial conditions are expressed as functions of

$$F_n = \left( \frac{1}{2\nu} \frac{d}{dt} \right)^n \xi, \quad (41)$$

where  $1 \gg F_1 \gg F_2 \gg F_n$ , and  $\xi = \ln(m\nu)$ . For our model, we set  $t = \eta_s$ ,  $\nu = k_s$ , and  $m = f$ . This condition implies that the function  $\xi = \ln(fk_s)$  changes slowly compared to  $\int 2k_s d\eta_s$ . In our numerical analysis, we utilize the adiabatic vacuum initial conditions up to the fourth order, applying this approximation until the truncation error becomes significant.

To illustrate how the couplings satisfy the adiabatic vacuum initial conditions as  $\eta_s \rightarrow -\infty$ , we examine their asymptotic behavior. In this limit, the scalar field  $\phi(\eta_s)$  typically grows large, as seen in Fig. 2. For the Gaussian coupling, the exponential term  $e^{-\phi^2/\beta^2}$  quickly tends to zero, leading to  $f_G(\phi(\eta_s)) \approx \frac{1}{4}$ . Similarly, for the Cauchy coupling, the term  $\frac{1}{1+(\phi/\beta)^2}$  also approaches zero, resulting in  $f_C(\phi(\eta_s)) \approx \frac{1}{4}$ . Thus, in the limit  $\eta_s \rightarrow -\infty$ , both coupling functions converge to a constant value of  $\frac{1}{4}$ , simplifying the initial conditions to:

$$A_k(\eta_s) \approx \sqrt{\frac{2}{k}} e^{-ik\eta_s}, \quad (42)$$

$$\Pi_k(\eta_s) \approx -i \sqrt{\frac{k}{8}} e^{-ik\eta_s}. \quad (43)$$

By studying these two extremes – the sharply decreasing Gaussian and the more gradually decreasing Cauchy coupling – we can effectively map the general behavior of such couplings. These represent limiting cases within a broader family of decreasing functions, allowing us to capture a wide range of possible dynamics and better understand the influence of different coupling behaviors on the evolution of the electromagnetic field in the model.

To accurately capture the dynamics of the electromagnetic field, we implement the adiabatic vacuum initial conditions specific to each coupling function within our numerical simulations. By initializing the field modes in their appropriate vacuum states and evolving them through the bounce, we ensure that the resulting predictions, including the magnetic field power spectrum, are robust. This method eliminates potential artifacts that could arise from improper initial conditions, while maintaining precision up to the point where the adiabatic approximation breaks down due to truncation errors.

## 4. NUMERICAL ANALYSIS OF PERTURBATIONS

### 4.1. Modes

We examine the time evolution of the magnetic and electric modes,  $|A_{sk}|^2$  and  $|\Pi_{sk}|^2$ , focusing on how the scale parameter  $\beta_G$  affects the magnetic modes for  $\alpha_G = 13.15$  and  $\alpha_G = 14.4$ . The values of  $\beta_G$  in Table 2 determine the transition point between the conformal and non-conformal regimes, defined by  $\phi_0 = \alpha_G \beta_G$ , which ranges from approximately 10 to 50. As shown in Fig. 2, this corresponds to the time interval  $\tau \in [-10, -5]$ .

We begin by plotting these modes because, in the absence of a non-trivial coupling, their magnitudes should remain constant, providing a baseline for comparison. Figure 4 illustrates the impact of  $\beta_G$  on the magnetic mode, while Fig. 5 demonstrates similar effects on the electric modes. Both figures focus on a fixed wavenumber,  $k = 4000$  (approximately 1 Mpc), although the overall behavior is consistent across larger scales. The uncoupled case, represented by the black line, serves as

Parameter	$\alpha_G$	$\beta_G$
Range	[13.15, 15.18]	[1, 2.99]

**Table 2**  
Range of coupling parameters  $\alpha_G$  and  $\beta_G$ .

a reference throughout the analysis. Table 2 provides a summary of the parameter ranges used in this study.

We first observe that while the Cauchy coupling evolves over time, its evolution occurs on a much smaller time scale compared to the Gaussian coupling, rendering its effects nearly imperceptible, partially because one needs a very small  $\beta_C$  in order to reach the conformal limit before the standard cosmological model evolution in the early universe begins to take place. Although the coupling parameters do influence the amplitude of the modes, the Cauchy coupling (depicted by the red curves) fails to generate notable magnetic or electric fields. While some amplification occurs, it remains insufficient to produce observable effects. For the same  $\alpha_G$ , the Cauchy coupling results in effects that are many orders of magnitude smaller than those of the Gaussian coupling. One could increase  $\alpha_C$  further to amplify the effects, but doing so would require an even smaller  $\beta_C$  to maintain the coupling within the conformal regime. We will explore these effects in more detail in Figs. 6 and 7.

Second, we observe that modes with Gaussian coupling (shown by the blue curves) evolve similarly to uncoupled modes in the distant past, as expected, given that the coupling is approximately constant in this regime. During the contraction phase, only the electric modes  $|\Pi_{sk}|^2$  increase, while the magnetic modes  $|A_{sk}|^2$  remain nearly constant. It is only during the expansion phase that the magnetic modes begin to grow. This behavior mirrors what is observed in other bouncing models coupled to gravity, as discussed in Frion et al. (2020). A broader Gaussian coupling (with larger  $\beta$ , indicated by the darker shades of blue) affects modes farther from the bounce, further amplifying the contrast between electric and magnetic mode evolution. This outcome is expected since larger  $\beta$  values cause the coupling to transition to the non-conformal regime earlier, allowing the modes to amplify sooner.

The behavior of the modes can be understood through the evolution of the Hamiltonian equations derived from Eq. (27):

$$\dot{A}_{sk} = \frac{\Pi_{sk}}{m}, \quad (44a)$$

$$\dot{\Pi}_{sk} = -m\nu^2 A_{sk}. \quad (44b)$$

In the super-Hubble regime, as the coupling increases, the effective mass  $m$  rises, leading to an increase in  $\Pi_{sk}$  while  $A_{sk}$  remains approximately constant. When the mode transitions into the sub-Hubble regime during the expanding phase, the increased momentum is transferred to the mode amplitude. This dynamic explains the behavior observed in Figs. 4 and 5. The key difference between the couplings lies in the timing of this variation: for the Cauchy coupling, it occurs very close to the bounce, whereas for the Gaussian coupling, the variation is spread over a longer period, due to the large difference between  $\beta_C$  and  $\beta_G$ , allowing for more gradual amplification.

cation.

#### 4.2. Power Spectra

Based on the previous analysis, we now investigate the dependence of the magnetic and electric power spectra,  $P_B$  and  $P_E$ , on the parameters  $\alpha_G$  and  $\beta_G$ . As shown in Fig. 6, the magnetic power spectra for the Cauchy modes exhibit minimal amplification, beginning near the baseline and increasing only marginally during the expansion phase. For  $\alpha_G = 13.15$  (left panel), the difference is a few orders of magnitude, rising to about 10 orders of magnitude for  $\alpha_G = 14.4$  (right panel). Consequently, the Cauchy coupling proves ineffective in generating primordial magnetic fields with significant amplitudes. In contrast, the Gaussian modes undergo substantial growth during the expansion phase, amplifying their magnetic power spectra to levels capable of explaining the observed magnetic fields on very large scales. In the following sections, we will further constrain the model's parameter space to explore the origins of these fields.

While the electric power spectra for both Cauchy and Gaussian modes exhibit similar qualitative behaviors, they differ in scale and amplitude. Specifically, both power spectra decrease during contraction ( $\tau < 0$ ) and increase during expansion ( $\tau > 0$ ). This is illustrated in Figure 7, where the primary distinction between the two types of couplings is their overall magnitude rather than the general trend of the mode evolution.

#### 4.3. Backreaction

Similar to magnetic power spectra, the electric power spectra dominate only significantly after the quantum-dominated regime around the bounce. Consequently, both electric and magnetic energy densities become important only in the classical regime, which leads us to conclude that no backreaction occurs during the quantum regime.

#### 4.4. Parameter Space

In Fig. 8, we illustrate the parameter space where our model produces viable seed magnetic fields. The green curve represents the upper bound of approximately 1 nG on the amplitude of seed magnetic fields, as constrained by various surveys, including observations from the CMB Ade et al. (2016), Ultra-High-Energy Cosmic Rays (UHECR) Bray and Scaife (2018), and 21-cm hydrogen lines Minoda et al. (2019). The orange curve denotes the lower bound derived from the non-detection of secondary GeV  $\gamma$ -rays around TeV blazars Taylor et al. (2011); Acciari et al. (2023), though this limit remains debated within the astrophysical community Broderick et al. (2012); Subramanian (2019) and should be interpreted with caution. Additionally, the blue curve represents the theoretical threshold required to initiate a galactic dynamo Subramanian et al. (1994); Martin and Yokoyama (2008). For the remainder of this study, we focus exclusively on the Gaussian coupling due to its viability in generating magnetic fields within these constraints.

The left and right panels of Fig. 8 display the parameter spaces for Set-1 and Set-2, respectively. Both cases exhibit a similar pattern, notably a sharp rise in  $\alpha_G$  as  $\beta_G$  nears 3, required to generate a magnetic seed field amplitude of 1 nG. This behavior is tied to the time evolution

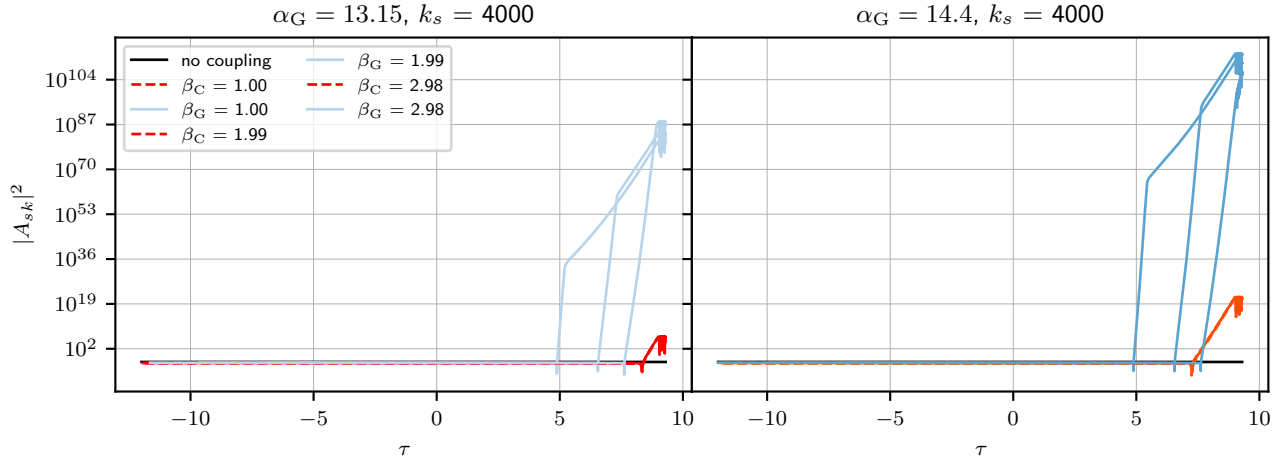


**Figure 4.** Time evolution of magnetic modes  $|A_{sk}|^2$ . Red curves represent modes with a Cauchy coupling, while blue curves represent modes with a Gaussian coupling. The black curve corresponds to the uncoupled case. The magnetic modes only begin to evolve significantly during the expansion phase ( $\tau > 0$ ). For both couplings, the amplitude of the modes increases with  $\alpha_G$ , with the amplification occurring as the modes become super-Hubble in the expanding phase.

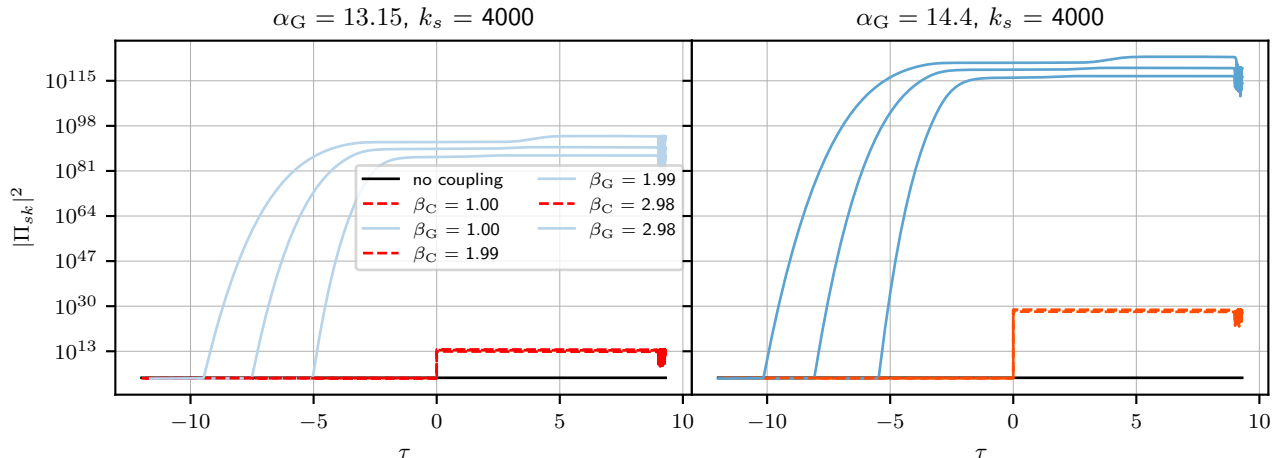


**Figure 5.** Time evolution of electric modes  $|\Pi_{sk}|^2$ . Red curves represent modes with a Cauchy coupling, and blue curves represent modes with a Gaussian coupling. The black curve corresponds to the uncoupled case. The electric modes start evolving in the contracting phase ( $\tau < 0$ ). For the Cauchy coupling, the momentum amplitude is enhanced relative to the no-coupling case near the bounce. The Gaussian modes follow a similar pattern but with varying amplification timescales. Both couplings yield larger amplitudes as  $\alpha_G$  increases.

of the magnetic field. In Fig. 9, we illustrate the magnetic field evolution over a brief interval ( $9.2 < \tau < 9.3$ ). By holding  $\beta_G$  fixed and increasing  $\alpha_G$  to achieve a 1 nG amplitude today, we see a sign change in the spectrum's slope. After this point, further increases in  $\alpha_G$  lead to only marginal changes in  $B_\lambda$ .

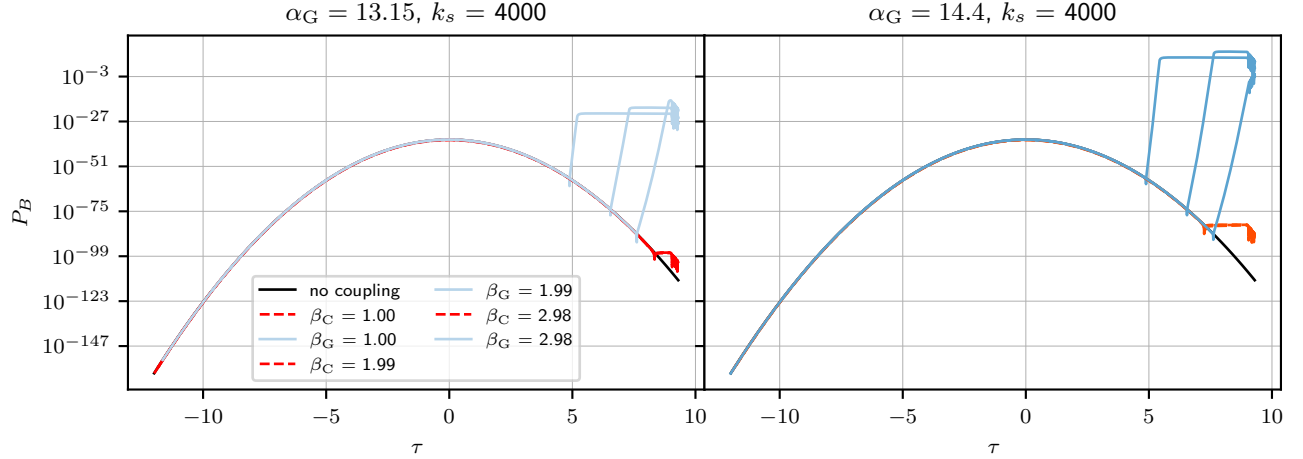
#### 4.5. Amplitude of Magnetic Fields

Figure 10 depicts the present-day amplitude of magnetic fields,  $B_{\lambda,0}$ , across different scales. The trends observed are consistent between Set-1 and Set-2. For super-Hubble modes, specifically in the range  $1 < k \leq 30$ , the magnetic fields follow a power-law distribution with a spectral index of  $n_B \simeq 4$ , largely independent of the specific values of  $\alpha_G$  and  $\beta_G$ . However, for modes within the Hubble radius, the spectral index  $n_B$  becomes more sensitive to  $\beta_G$ . When  $\beta_G$  is between 1 and 2.8, the average scalar index  $n_B$  decreases from 4 to approximately 3. Beyond this range, particularly for  $\beta_G > 2.8$ , the slope undergoes a more pronounced shift, dropping to as low as  $n_B = 0.5$  for  $\beta_G = 2.99$ , though it remains positive.

age scalar index  $n_B$  decreases from 4 to approximately 3. Beyond this range, particularly for  $\beta_G > 2.8$ , the slope undergoes a more pronounced shift, dropping to as low as  $n_B = 0.5$  for  $\beta_G = 2.99$ , though it remains positive.

## 5. DISCUSSION

The results of this study suggest that a bouncing universe together with a coupling between the scalar field  $\phi$  which sources the background model and the electromagnetic field can lead to sufficient primordial magnetogenesis in accordance with observations. We explored the evolution of the electromagnetic field starting from the contraction phase, through the bounce, and into the expansion phase, beginning with an initial adiabatic vacuum state. Our numerical analysis reveals that magnetic fields on a 1 Mpc scale can achieve amplitudes consistent with current cosmological observations. This is signifi-



**Figure 6.** Evolution of the magnetic power spectrum  $P_B$  with time for modes  $k = 4,000$ . The colors and parameters are the same as for the modes in figures 4 and 5. A Cauchy coupling is unable to explain the origin or large-scale magnetic fields, while a Gaussian coupling is an efficient way of producing strong seed magnetic fields.

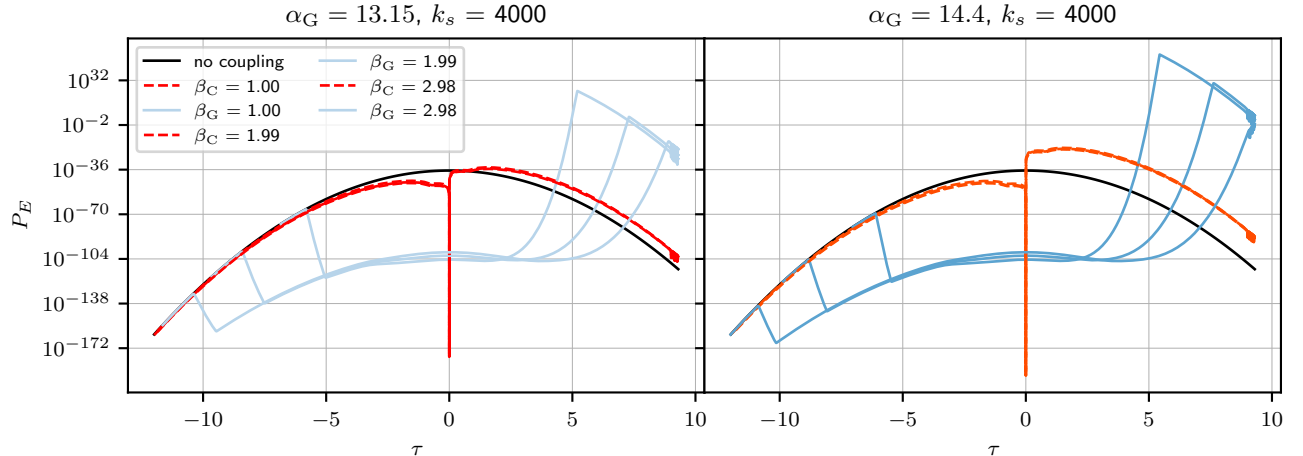


**Figure 7.** Evolution of the electric power spectrum  $P_E$  with time for modes  $k = 4,000$ . The colors and parameters are the same as for the modes in figures 4 and 5. Both the Cauchy and Gaussian couplings see their amplitude decreasing during contraction ( $\tau < 0$ ) and increasing during expansion ( $\tau > 0$ ), though the amplification is much stronger in the Gaussian case.

cant because it shows that, in the presence of the coupling, the magnetic fields generated during the bounce are sufficiently strong to serve as seeds for further amplification by dynamo mechanisms in astrophysical structures, supporting the potential of this model to explain the observed magnetic fields in the universe.

Two critical parameters in the model are  $\alpha_G$  and  $\beta_G$ , which play a pivotal role in shaping the results. The parameter  $\beta_G$  determines the width of the coupling functions, while  $\alpha_G$  sets the coupling amplitude. The value of  $\beta_G$  controls the duration of the coupling's influence, with larger values extending the coupling's effect over a longer period around the bounce. Our analysis shows that a range of  $\beta_G$  values between 1 and 2.99 can generate magnetic fields consistent with current observations. In particular, values near the upper bound,  $\beta_G \approx 2.99$ , yield stronger magnetic fields. This occurs because higher  $\beta_G$  values prolong the interaction between the scalar field  $\phi$  and the electromagnetic field, leading to greater energy

transfer to the magnetic field. This not only amplifies the magnetic field's strength but also smooths and extends the oscillations in the power spectrum over time.

The parameter  $\alpha_G$  influences the strength of the coupling between the scalar field  $\phi$  and the electromagnetic field. Larger values of  $\alpha_G$  result in greater amplification of the magnetic modes by intensifying the interaction between  $\phi$  and the electromagnetic field. Our results show that for  $\alpha_G$  in the range of 12.7 to 15.18, the generated magnetic fields align with observational limits. As  $\beta_G$  approaches 3, higher values of  $\alpha_G$  are necessary to achieve a magnetic field amplitude of 1 nG today. This is because a stronger coupling (higher  $\alpha_G$ ) provides additional energy for amplifying the magnetic fields to match cosmological observations. Moreover, varying  $\alpha_G$  affects the power spectrum's slope and the degree of amplification, leading to significant changes in the power spectrum's qualitative features, such as the prominence of peaks and troughs.

Another important aspect are the oscillations observed

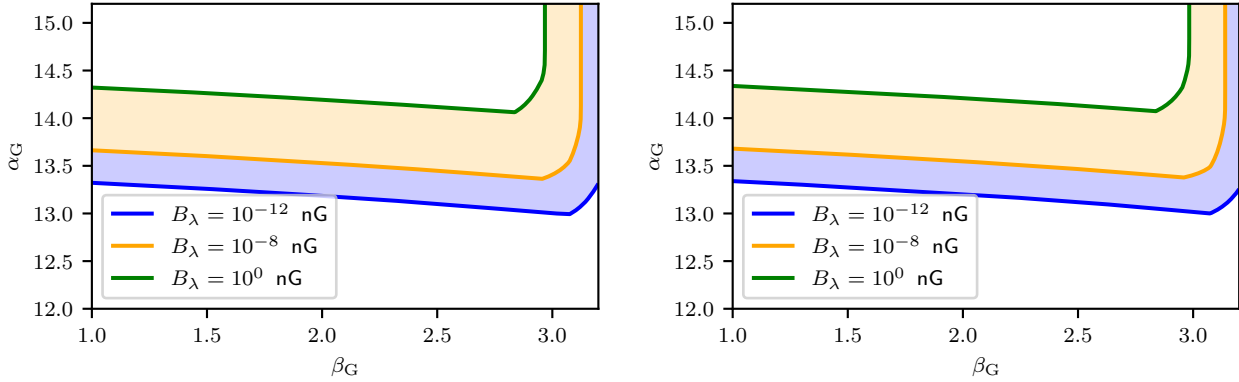


**Figure 8.** Viable parameter space  $(\alpha_G, \beta_G)$  for the generation of primordial magnetic fields compatible with observations. The parameter space for Set-1 is on the left, for Set-2 on the right. The green curve corresponds to the upper constraints on magnetic field amplitudes  $\approx 1$  nG, the orange curve to lower constraints from  $\gamma$ -rays, and the blue curve a lower threshold to initiate dynamo amplification. The orange region contains values of  $\alpha_G$  and  $\beta_G$  leading to viable magnetic seed fields, and overlaps with the dynamo (blue) region. For both sets, there is a sharp increase in the value of  $\alpha_G$  needed to obtain a magnetic field amplitude of 1 nG when  $\beta_G \rightarrow 3$ .

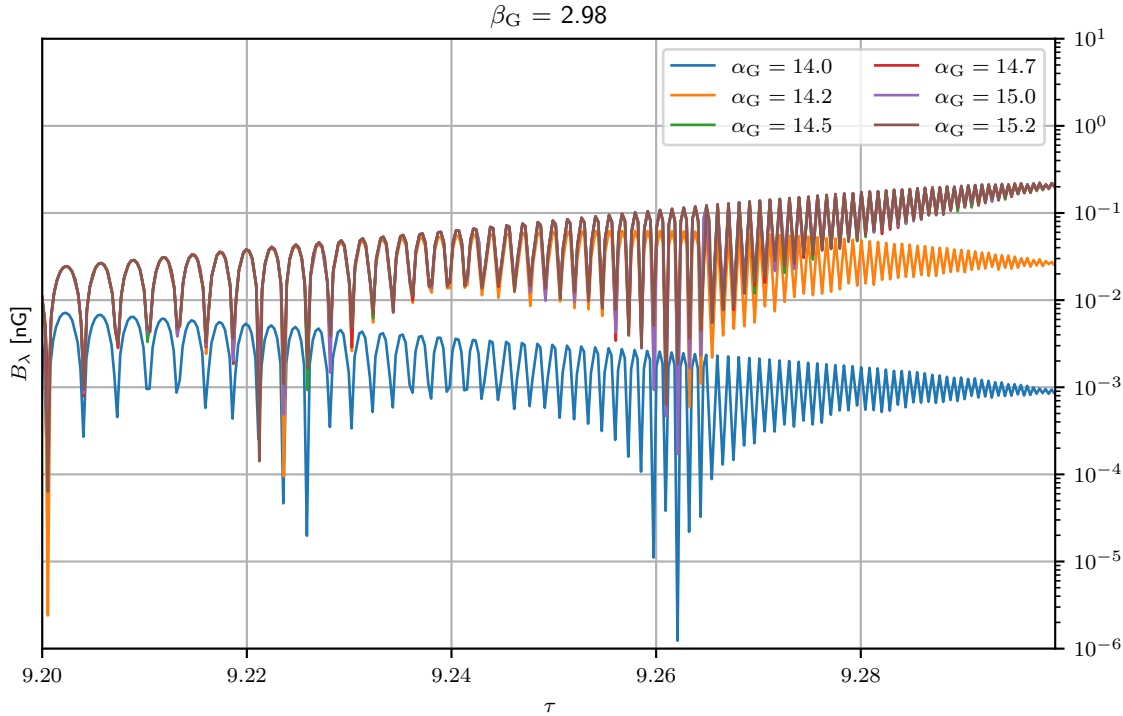


**Figure 9.** At fixed  $\beta_G$ , increasing  $\alpha_G$  ends up changing the slope of the magnetic field. Starting with a negative slope for lower values of  $\alpha_G$  (blue curve) and increasing  $\alpha_G$  changes the sign of the slope. In this example, for  $\alpha_G > 14.48$ , all curves are superposed. Therefore, there is a saturation mechanism related to the sign of the slope.

at the end of the evolution of the power spectra. These oscillations begin when the modes enter the Hubble radius and start behaving like typical electromagnetic waves, as they are no longer super-Hubble. At this point, the oscillations arise purely from the dynamics of the electromagnetic fields, rather than interactions with other matter components.

In the context of primordial magnetogenesis in a bouncing universe model, the issue of backreaction – i.e., the influence of the generated magnetic fields on the dynamics of the universe – does not present itself as a significant problem. The energy density of the magnetic fields  $\rho_B$  must be compared with the background

energy density  $\rho_\phi$  to assess the impact of backreaction. In our model, we verify that  $\rho_B$  remains significantly smaller than  $\rho_\phi$  throughout the entire cosmological evolution considered. Specifically, the energy density of the generated magnetic fields  $\rho_B$  is given by

$$\rho_B = \int_{k_{\min}}^{k_{\max}} \frac{d \ln k}{8\pi} P_B(k),$$

where  $P_B(k)$  is the magnetic field power spectrum, calculated numerically. Comparing this expression with the

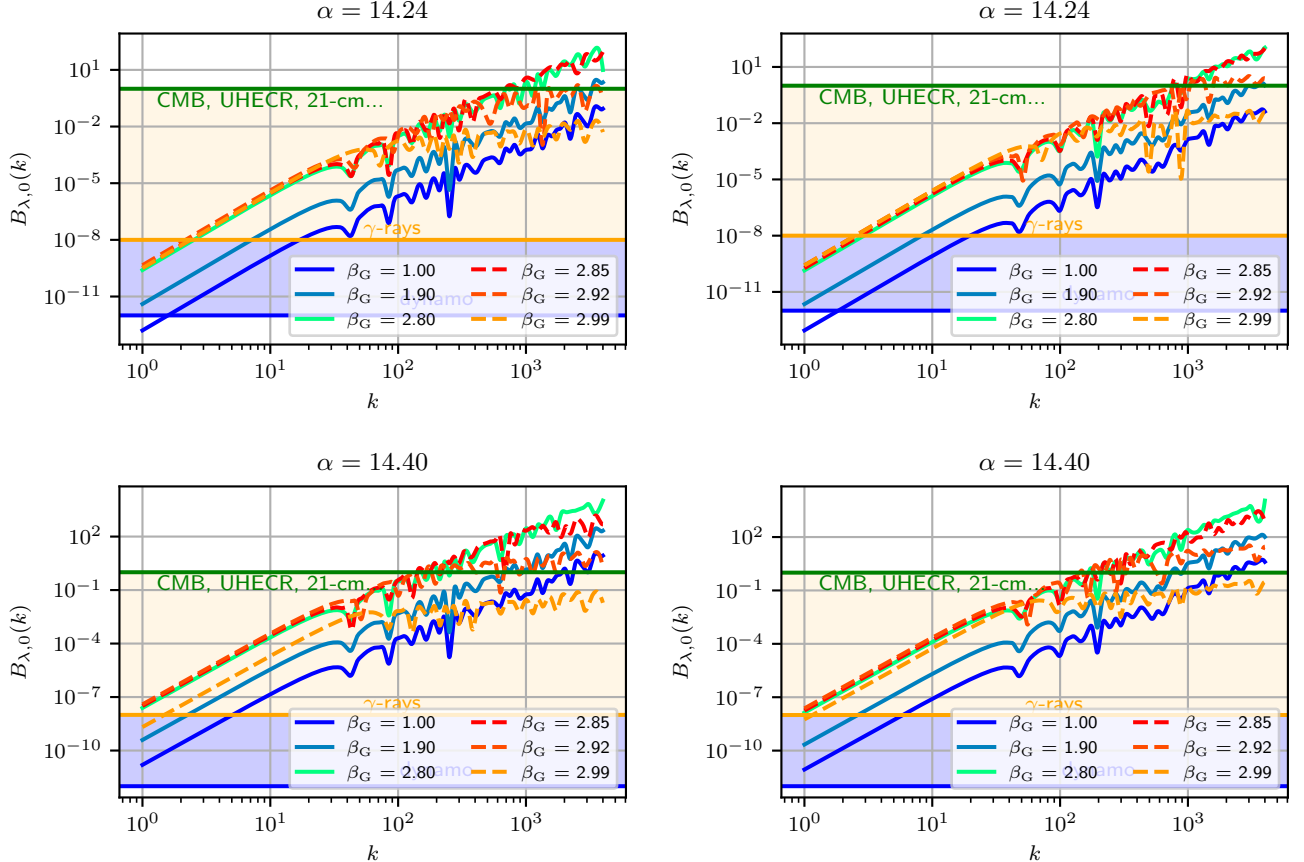


**Figure 10.** Evolution of the amplitude of magnetic fields today with the scale. We keep the same color code for bounds on the amplitude as in figure 8. Figures for Set-1 are on the left, for Set-2 on the right. For all values of  $\alpha_G$  and  $\beta_G$ , magnetic fields have a blue-tilted spectral index  $n_B$ . On the largest scales  $0 < k \leq 30$ ,  $n_B = 4$  always. For scales  $k > 30$ , we have  $n_B \simeq 3$  while  $1 < \beta < 2.8$ , and  $0.5 < n_B < 3$  for  $\beta > 2.8$ .

background energy density  $\rho_\phi$ , which is given by:

$$\rho_\phi = \frac{1}{2} \dot{\phi}^2 + V(\phi).$$

The terms that dominate  $\rho_\phi$  depend on the phase of the universe. During the contraction phase, the kinetic term  $\frac{1}{2} \dot{\phi}^2$  tends to dominate, making  $\rho_\phi \propto e^{-6\alpha}$ . In the expansion phase, the energy density of the scalar field is influenced by the contribution of the potential  $V(\phi)$ , which becomes more relevant. This dependence of the background energy density on the scale factor, along with the Planck length, corroborates the stability of the model concerning the back-reaction problem. The same is true concerning the energy density of electric field.

For example, considering typical values of the potential  $V(\phi)$  and the evolution of the scale factor  $a(t)$ , the energy density  $\rho_\phi$  can vary from  $10^{-12} \text{ GeV}^4$  during the contraction phase to  $10^{-9} \text{ GeV}^4$  in the expansion phase. These values are widely accepted in the cosmological literature and show that, even with the amplification of the magnetic fields, the energy density  $\rho_B$  remains well below  $\rho_\phi$ , ensuring that backreaction is not a problem in this scenario.

## 6. CONCLUSIONS

In this work, we presented the generation of primordial magnetic fields in the context of a cosmological bounce through a coupling between the electromagnetic field and a scalar field. We considered a homogeneous and isotropic background filled with a scalar field which behaves as a pressureless (dark) matter fluid in the asymptotic contracting phase, as a stiff-matter fluid near the bounce, and as dark energy in some period of the expanding phase. The bounce is produced by quantum effects described using the de Broglie-Bohm quantum theory, motivated by the inconsistency of using standard quantum mechanics in quantum cosmology Pinto-Neto and Fabris (2013). The background model has scalar cosmological perturbations in accordance with CMB observations, see Ref. Bacalhau et al. (2018) for details.

Some advantages of the bounce magnetogenesis are the absence of the strong coupling problem and back-reaction. The model is characterized by three main parameters: the coupling amplitude  $\alpha_G$ , the width of the coupling function  $\beta_G$ , and the specific form of the coupling (Gaussian or Cauchy), which have been explored, leading to relevant primordial magnetic fields which can source the observed magnetic fields observed in galaxies and clusters. Only the Gaussian coupling, with its intrinsic abrupt fall-off, can yield such magnetic fields. The full electromagnetic field evolves from fluctuations

of an adiabatic vacuum properly defined in the far past of the cosmological model either for the Gaussian and Cauchy couplings.

The inclusion of theoretical limits on gravitational wave production, see Ref. [Caprini and Durrer \(2001\)](#) will be investigated in the future. This will be even more relevant with the upcoming observations from LISA [Caprini et al. \(2009\)](#); [Caprini and Figueroa \(2018\)](#); [Saga et al. \(2018b\)](#); [Roper Pol et al. \(2019\)](#).

A second point of interest would be to consider other possible backreaction effects. It has been shown recently that vacuum polarization in a dielectric medium, the so-called Schwinger effect, increases the conductivity of the medium and subsequently halts the production of the magnetic field [Sobol et al. \(2018, 2019\)](#); [Sharma et al. \(2017, 2018\)](#); [Shakeri et al. \(2019\)](#). This effect could lead to weaker magnetic fields than expected and could further constrain our model. It is important to investigate how these interactions affect the evolution of the magnetic field and whether there are ways to mitigate these effects to preserve the viability of the bounce magnetogenesis model.

As a possible extension of our work, other non-minimal couplings between the electromagnetic field and the scalar field can be explored. For example, couplings dependent on other functional forms of the scalar field or couplings that vary in time may provide new perspectives on the generation of primordial magnetic fields.

We leave these questions for future work, encouraging the exploration of new models and the consideration of additional effects that may impact the generation and evolution of primordial magnetic fields in the context of a cosmological bounce.

## REFERENCES

V. A. Acciari et al. A lower bound on intergalactic magnetic fields from time variability of 1ES 0229+200 from MAGIC and Fermi/LAT observations. *Astron. Astrophys.*, 670:A145, 2023. doi:10.1051/0004-6361/202244126.

P.A.R. Ade et al. Planck 2015 results. XIX. Constraints on primordial magnetic fields. *Astron. Astrophys.*, 594:A19, 2016. doi:10.1051/0004-6361/201525821.

Peter Adshead, John T. Giblin, Timothy R. Scully, and Evangelos I. Sfakianakis. Magnetogenesis from axion inflation. *JCAP*, 10:039, 2016. doi:10.1088/1475-7516/2016/10/039.

Anna Paula Bacalhau, Nelson Pinto-Neto, and Sandro Dias Pinto Vitenti. Consistent Scalar and Tensor Perturbation Power Spectra in Single Fluid Matter Bounce with Dark Energy Era. *Phys. Rev. D*, 97(8):083517, 2018. doi:10.1103/PhysRevD.97.083517.

Kazuharu Bamba and Misao Sasaki. Large-scale magnetic fields in the inflationary universe. *JCAP*, 0702:030, 2007. doi:10.1088/1475-7516/2007/02/030.

Paramita Barai and Elisabete M. de Gouveia Dal Pino. Large-Scale Diffuse Intergalactic Magnetic Fields Constraints with the Cherenkov Telescope Array. In *Proceedings of Talk presented at the IAU Focus Meeting FM8: "New Insights in Extragalactic Magnetic Fields"*, held at the IAU General Assembly - Vienna, 2018 August 29-31, 11 2018.

Neil D. Barrie. Big Bounce Baryogenesis. *JCAP*, 08:008, 2020. doi:10.1088/1475-7516/2020/08/008.

Thorsten J. Battfeld and Robert Brandenberger. Vector perturbations in a contracting universe. *Phys. Rev.*, D70:121302, 2004. doi:10.1103/PhysRevD.70.121302.

Rainer Beck. Magnetic fields in galaxies. *Space Science Reviews*, 166(1-4):215–230, 2012. doi:10.1007/s11214-011-9782-z.

Rainer Beck and Richard Wielebinski. Magnetic Fields in the Milky Way and in Galaxies. *Planets, Stars and Stellar Systems*, pages 641–723, 2 2013. doi:10.1007/978-94-007-5612-0“13.

J.D. Bray and A.M.M. Scaife. An upper limit on the strength of the extragalactic magnetic field from ultra-high-energy cosmic-ray anisotropy. *Astrophys. J.*, 861(1):3, 2018. doi:10.3847/1538-4357/aac777.

Avery E. Broderick, Philip Chang, and Christoph Pfrommer. The Cosmological Impact of Luminous TeV Blazars I: Implications of Plasma Instabilities for the Intergalactic Magnetic Field and Extragalactic Gamma-Ray Background. *Astrophys. J.*, 752:22, 2012. doi:10.1088/0004-637X/752/1/22.

L. Campanelli, P. Cea, G. L. Fogli, and L. Tedesco. Inflation-Produced Magnetic Fields in  $R^n F^2$  and  $IF^2$  models. *Phys. Rev.*, D77:123002, 2008. doi:10.1103/PhysRevD.77.123002.

Chiara Caprini and Ruth Durrer. Gravitational wave production: A Strong constraint on primordial magnetic fields. *Phys. Rev. D*, 65:023517, 2001. doi:10.1103/PhysRevD.65.023517.

Chiara Caprini and Daniel G. Figueroa. Cosmological Backgrounds of Gravitational Waves. *Class. Quant. Grav.*, 35(16):163001, 2018. doi:10.1088/1361-6382/aac608.

Chiara Caprini, Ruth Durrer, and Geraldine Servant. The stochastic gravitational wave background from turbulence and magnetic fields generated by a first-order phase transition. *JCAP*, 0912:024, 2009. doi:10.1088/1475-7516/2009/12/024.

Diogo C. F. Celani, Nelson Pinto-Neto, and Sandro D. P. Vitenti. Particle Creation in Bouncing Cosmologies. *Phys. Rev. D*, 95(2):023523, 2017. doi:10.48550/arXiv.1610.04933.

Jie-Wen Chen, Chong-Huan Li, Yu-Bin Li, and Mian Zhu. Primordial magnetic fields from gravitationally coupled electrodynamics in nonsingular bounce cosmology. *Sci. China Phys. Mech. Astron.*, 61(10):100411, 2018. doi:10.1007/s11433-018-9211-5.

J. Chluba et al. Spectral Distortions of the CMB as a Probe of Inflation, Recombination, Structure Formation and Particle Physics: Astro2020 Science White Paper. *Bull. Am. Astron. Soc.*, 51(3):184, 2019.

Debika Chowdhury, L. Sriramkumar, and Rajeev Kumar Jain. Duality and scale invariant magnetic fields from bouncing universes. *Phys. Rev.*, D94(8):083512, 2016. doi:10.1103/PhysRevD.94.083512.

Debika Chowdhury, L. Sriramkumar, and Marc Kamionkowski. Cross-correlations between scalar perturbations and magnetic fields in bouncing universes. *JCAP*, 1901:048, 2019. doi:10.1088/1475-7516/2019/01/048.

R Colistete Jr, JC Fabris, and N Pinto-Neto. Gaussian superpositions in scalar-tensor quantum cosmological models. *Physical Review D*, 62(8):083507, 2000.

P.'C.'M. Delgado, M.'B. Jesus, N. Pinto-Neto, T. Mourão, and G.'S. Vicente. Baryogenesis in cosmological models with symmetric and asymmetric quantum bounces. *Phys. Rev. D*, 102:063529, 2020. doi:10.1103/PhysRevD.102.063529.

Paul A.M. Dirac. Generalized Hamiltonian dynamics. *Can. J. Math.*, 2:129–148, 1950. doi:10.4153/CJM-1950-012-1.

Ruth Durrer and Andrii Neronov. Cosmological Magnetic Fields: Their Generation, Evolution and Observation. *Astron. Astrophys. Rev.*, 21:62, 2013. doi:10.1007/s00159-013-0062-7.

Razieh Emami, Hassan Firouzjahi, and M. Sadegh Movahed. Inflation from Charged Scalar and Primordial Magnetic Fields? *Phys. Rev.*, D81:083526, 2010. doi:10.1103/PhysRevD.81.083526.

E. Frion, N. Pinto-Neto, S. D. P. Vitenti, and S. E. Perez Bergliaffa. Primordial Magnetogenesis in a Bouncing Universe. *Phys. Rev. D*, 101(10):103503, 2020. doi:10.1103/PhysRevD.101.103503.

Imogen P C Heard and David Wands. Cosmology with positive and negative exponential potentials. *Classical and Quantum Gravity*, 19(21):5435, 2002. doi:10.1088/0264-9381/19/21/309.

Masahiro Kawasaki and Motohiko Kusakabe. Updated constraint on a primordial magnetic field during big bang nucleosynthesis and a formulation of field effects. *Phys. Rev. D*, 86:063003, 2012. doi:10.1103/PhysRevD.86.063003.

Ratna Koley and Sidhartha Samtani. Magnetogenesis in Matter - Ekpyrotic Bouncing Cosmology. *JCAP*, 1704(04):030, 2017. doi:10.1088/1475-7516/2017/04/030.

Kerstin E. Kunze. Large scale magnetic fields from gravitationally coupled electrodynamics. *Phys. Rev.*, D81:043526, 2010. doi:10.1103/PhysRevD.81.043526.

Kerstin E. Kunze. Completing magnetic field generation from gravitationally coupled electrodynamics with the curvaton mechanism. *Phys. Rev.*, D87(6):063505, 2013. doi:10.1103/PhysRevD.87.063505.

Natacha Leite and Petar Pavlović. Magnetogenesis in Cyclical Universe. *Class. Quant. Grav.*, 35(21):215005, 2018. doi:10.1088/1361-6382/aae2d6.

Jerome Martin and Jun'ichi Yokoyama. Generation of Large-Scale Magnetic Fields in Single-Field Inflation. *JCAP*, 01:025, 2008. doi:10.1088/1475-7516/2008/01/025.

Federico Agustín Membela. Primordial magnetic fields from a non-singular bouncing cosmology. *Nucl. Phys.*, B885:196–224, 2014. doi:10.1016/j.nuclphysb.2014.05.018.

Teppei Minoda, Hiroyuki Tashiro, and Tomo Takahashi. Insight into primordial magnetic fields from 21-cm line observation with EDGES experiment. *Mon. Not. Roy. Astron. Soc.*, 488(2):2001–2005, 2019. doi:10.1093/mnras/stz1860.

Meysam Motaharfar and Parampreet Singh. Anisotropic non-singular quantum bounce as a seesaw and amplification mechanism for magnetic fields. *arXiv e-prints*, 6 2024.

Mariana Penna-Lima, Nelson Pinto-Neto, and Sandro D. P. Vitenti. New formalism to define vacuum states for scalar fields in curved spacetimes. *Phys. Rev. D*, 107(6):065019, 2023. doi:10.1103/PhysRevD.107.065019.

Patrick Peter and Nelson Pinto-Neto. Cosmology without inflation. *Phys. Rev. D*, 78:063506, 2008. doi:10.1103/PhysRevD.78.063506.

N. Pinto-Neto and J.C. Fabris. Quantum cosmology from the de Broglie-Bohm perspective. *Class. Quant. Grav.*, 30:143001, 2013. doi:10.1088/0264-9381/30/14/143001.

Levon Pogosian and Alex Zucca. Searching for Primordial Magnetic Fields with CMB B-modes. *Class. Quant. Grav.*, 35(12):124004, 2018. doi:10.1088/1361-6382/aac398.

Peng Qian, Yi-Fu Cai, Damien A. Easson, and Zong-Kuan Guo. Magnetogenesis in bouncing cosmology. *Phys. Rev.*, D94(8):083524, 2016. doi:10.1103/PhysRevD.94.083524.

J. Quintin, Y. Cai, and R. H. Brandenberger. Matter creation in a nonsingular bouncing cosmology. *Phys. Rev. D*, 90(2):063507, 2014. doi:10.1103/PhysRevD.90.063507.

Alberto Roper Pol, Sayan Mandal, Axel Brandenburg, Tina Kahnashvili, and Arthur Kosowsky. Numerical Simulations of Gravitational Waves from Early-Universe Turbulence. *arXiv e-prints*, 2019.

Shohei Saga, Hiroyuki Tashiro, and Shuichiro Yokoyama. Magnetic reheating. *Mon. Not. Roy. Astron. Soc.*, 474(1):L52–L55, 2018a. doi:10.1093/mnrasl/slx195.

Shohei Saga, Hiroyuki Tashiro, and Shuichiro Yokoyama. Limits on primordial magnetic fields from direct detection experiments of gravitational wave background. *Phys. Rev. D*, 98(8):083518, 2018b. doi:10.1103/PhysRevD.98.083518.

J. M. Salim, N. Souza, Santiago E. Perez Bergliaffa, and T. Prokopec. Creation of cosmological magnetic fields in a bouncing cosmology. *JCAP*, 0704:011, 2007. doi:10.1088/1475-7516/2007/04/011.

Oleg Savchenko and Yuri Shtanov. Magnetogenesis by non-minimal coupling to gravity in the Starobinsky inflationary model. *JCAP*, 1810:040, 2018. doi:10.1088/1475-7516/2018/10/040.

A. Scardua, L.'F. Guimarães, N. Pinto-Neto, and G.'S Vicente. Fermion production in bouncing cosmologies. *Phys. Rev. D*, 98:083505, 2018. doi:10.1103/PhysRevD.98.083505.

Soroush Shakeri, Mohammad Ali Gorji, and Hassan Firouzjahi. Schwinger Mechanism During Inflation. *Phys. Rev.*, D99(10):103525, 2019. doi:10.1103/PhysRevD.99.103525.

Ramkishor Sharma, Sandhya Jagannathan, T. R. Seshadri, and Kandaswamy Subramanian. Challenges in Inflationary Magnetogenesis: Constraints from Strong Coupling, Backreaction and the Schwinger Effect. *Phys. Rev.*, D96(8):083511, 2017. doi:10.1103/PhysRevD.96.083511.

Ramkishor Sharma, Kandaswamy Subramanian, and T. R. Seshadri. Generation of helical magnetic field in a viable scenario of inflationary magnetogenesis. *Phys. Rev.*, D97(8):083503, 2018. doi:10.1103/PhysRevD.97.083503.

O. O. Sobol, E. V. Gorbar, M. Kamarpour, and S. I. Vilchinskii. Influence of backreaction of electric fields and Schwinger effect on inflationary magnetogenesis. *Phys. Rev.*, D98(6):063534, 2018. doi:10.1103/PhysRevD.98.063534.

O. O. Sobol, E. V. Gorbar, and S. I. Vilchinskii. Backreaction of electromagnetic fields and the Schwinger effect in pseudoscalar inflation magnetogenesis. *Phys. Rev.*, D100(6):063523, 2019. doi:10.1103/PhysRevD.100.063523.

L. Sriramkumar, Kumar Atmjeet, and Rajeev Kumar Jain. Generation of scale invariant magnetic fields in bouncing universes. *JCAP*, 1509(09):010, 2015. doi:10.1088/1475-7516/2015/09/010.

K Subramanian, D Narasimha, and S Chitre. Thermal generation of cosmological seed magnetic fields in ionization fronts. *Mon. Not. Roy. Astron. Soc.*, 271(1):L15–L18, 11 1994. ISSN 0035-8711. doi:10.1093/mnras/271.1.L15.

Kandaswamy Subramanian. From primordial seed magnetic fields to the galactic dynamo. *Galaxies*, 7(2):47, 2019. doi:10.3390/galaxies7020047.

A.M. Taylor, I. Vovk, and A. Neronov. Extragalactic magnetic fields constraints from simultaneous GeV-TeV observations of blazars. *Astron. Astrophys.*, 529:A144, 2011. doi:10.1051/0004-6361/201116441.

Sagarika Tripathy, Debika Chowdhury, Rajeev Kumar Jain, and L. Sriramkumar. Challenges in the choice of the nonconformal coupling function in inflationary magnetogenesis. *Phys. Rev. D*, 105(6):063519, 2022. doi:10.1103/PhysRevD.105.063519.

Michael S. Turner and Lawrence M. Widrow. Inflation-produced, large-scale magnetic fields. *Phys. Rev. D*, 37:2743–2754, May 1988. doi:10.1103/PhysRevD.37.2743.

Alex Zucca, Yun Li, and Levon Pogosian. Constraints on Primordial Magnetic Fields from Planck combined with the South Pole Telescope CMB B-mode polarization measurements. *Phys. Rev.*, D95(6):063506, 2017. doi:10.1103/PhysRevD.95.063506.

This paper was built using the Open Journal of Astrophysics L<sup>A</sup>T<sub>E</sub>X template. The OJA is a journal which

provides fast and easy peer review for new papers in the **astro-ph** section of the arXiv, making the reviewing process simpler for authors and referees alike. Learn more at <http://astro.theoj.org>.